PAPER

Flexible devices fabricated by a plate-to-roll nanoimprint lithography system

To cite this article: Kai Xu *et al* 2019 *Nanotechnology* **30** 075301

View the article online for updates and enhancements.

Recent citations

- Metal mesh electrode array fabricated by plate-to-roll nanoimprint lithography
Kai Xu *et al*

- Optical polarization measurement for measuring deflection radius of the optically anisotropic flexible-polymeric substrate
Jiong-Shiun Hsu and Wen-Pin Juan

- Flexible touch sensor fabricated by double-sided nanoimprint lithography metal transfer
Muyi Yang *et al*

This content was downloaded from IP address 115.154.161.44 on 14/05/2021 at 09:52

IOP Publishing Nanotechnology
Nanotechnology 30 (2019) 075301 (5pp) https://doi.org/10.1088/1361-6528/aaf26f

Flexible devices fabricated by a plate-to-roll nanoimprint lithography system

Kai Xu, Huiwen Luo, Jin Qin, Muyi Yang, Songpo Guo and Liang Wang

University of Science and Technology of China, Anhui Key Laboratory of Optoelectronic Science and Technology, Department of Optics and Optical Engineering, No.96, JinZhai Road Baohe District, Hefei, Anhui, People's Republic of China, 230026

E-mail: lwang121@ustc.edu.cn

Received 12 August 2018, revised 7 November 2018
Accepted for publication 20 November 2018
Published 14 December 2018

Abstract

A plate-to-roll nanoimprint lithography (P2RNIL) system has been developed to realize a high-speed, large-scale and high-resolution nanoimprint process. Imprinted patterns have been achieved with a linewidth of less than 75 nm at a speed of 22 $cm^2 s^{-1}$ on flexible substrate. To improve the quality of the imprinted patterns, we have proposed a compliant mechanism which can realize passive alignment and minimize the lateral displacement between template and substrate. Finite element analysis of this compliant mechanism was carried out. By using the P2RNIL system, wire-grid polarizers (up to a 10 030:1 extinction ratio and up to 88% transmittance) and transparent metal electrodes whose performance is in good accordance with simulated results were successfully fabricated.

Supplementary material for this article is available online

Keywords: polymer, physical aging, structural relaxation, polymer physics, differential scanning calorimetry

(Some figures may appear in colour only in the online journal)

1. Introduction

Flexible devices have attracted extensive interest because they can offer a wide variety of novel applications, such as flexible displays [1], flexible solar cells [2], and some other stretchable electronics [3]. A wire-grid polarizer (WGP), which is a series of metallic gratings deposited on a dielectric substrate, is able to achieve the high-contrast polarization needed in liquid crystal displays and projected displays [4, 5]. The performance of a WGP is mainly determined by the transmittance and extinction ratios, which can be improved by adjusting the linewidth and aspect ratio of the metallic gratings. A high-performance WGP can easily be fabricated on a rigid substrate, but it becomes more challenging when flexible WGPs with good uniformity and large-format patterns are demanded. A transparent metal electrode (TME), as a replacement for indium-doped tin oxide (ITO), in the form of a periodically arranged metal mesh deposited on dielectric substrates, is promising for use in flexible displays and flexible solar cells. This kind of structure has characteristics of high optical transmittance and good electrical conductivity, which an ITO electrode cannot provide. However, it remains a challenge to fabricate a TME on a flexible substrate at low cost and with high quality.

The production process of WGPs and TMEs on rigid substrates is relatively mature, since these substrates are compatible with well-developed micro-nano manufacturing processes such as photolithography and dry etching. However, for the flexible substrate, nanoimprint lithography (NIL) shows great potential, not only because it can achieve resolution beyond the optical diffraction limit [6–8], but also because large-format patterns can be manufactured singly or in continuous mode. Due to these advantages, NIL has been rapidly developed from plate-to-plate nanoimprint lithography (P2PNIL) to roller-type NIL such as roll-to roll nanoimprint lithography (R2RNIL) [9–12] and roll-to plate nanoimprint lithography (R2PNIL) [13, 14] to fulfill the demands generated by recent developments in flexible electronics industries [15, 16]. The development of NIL has gained great momentum in the past few years, with numerous applications in areas such as organic or multi-junction

 © 2018 IOP Publishing Ltd Printed in the UK

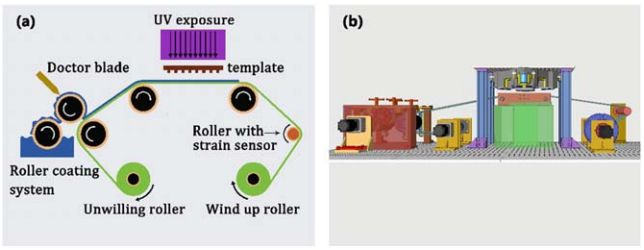

Figure 1. (a) A schematic of the P2RNIL process. (b) A 3D model of our P2RNIL system.

solar cells [17, 18], micro-electro-mechanical systems manufacturing [19], and biology [20]. P2PNIL is designed to realize high-resolution nanostructure transfer with a plate template which is easy to fabricate, but it offers only low throughput since it cannot work continuously. R2RNIL uses a cylinder template and a roll-to-roll process to realize continuous imprinting, which improves productivity significantly, but the high-resolution cylinder template is difficult to fabricate and can easily be abraded during the process. Both P2PNIL and R2RNIL have inevitable drawbacks which limit their use in the manufacture of flexible devices [12].

In this study, we developed a plate-to-roll nanoimprint lithography (P2RNIL) system which uses a plate template and flexible substrates fed and retrieved by the roller-based system. A compliant mechanism is designed and manufactured to ensure that the template is parallel to the substrate during the imprint process, which is an essential condition for avoiding large area vacancy [21]. The plate-type template shows great potential to reduce the difficulties encountered in fabricating and maintaining the roller templates required for R2RNIL. Gratings of less than 75 nm at room temperature and at a speed of 22 $cm^2\ s^{-1}$ have been achieved. A WGP and TME were successfully fabricated on flexible substrate. The performance of the WGP and TME were tested by measuring their transmittance, extinction ratio, and sheet resistance.

2. Materials and methods

2.1. The P2RNIL method

A schematic of the P2RNIL system and the 3D model of the equipment are shown in figure 1. The imprinting process starts at the two-roller coating system, where UV-curable resist (PhiChem, KY90F9-19) is transferred by the relative rotation of the two rollers, while a doctor blade is used to control the thickness of the resist. The thickness can be varied from 1 μm to 10 μm. The polyethylene terephthalate (PET) is driven by a wind-up roller and stops when the part carried with the resist is directly below the template. A strain sensor is used to maintain constant tension on the PET to ensure fidelity of duplication.

During the imprinting process, an imprint head moves downwards to force the template into contact with the substrate. The imprint head module plays a critical role in P2RNIL, since it directly influences the quality of imprinted patterns. In this process, the template and the substrate should

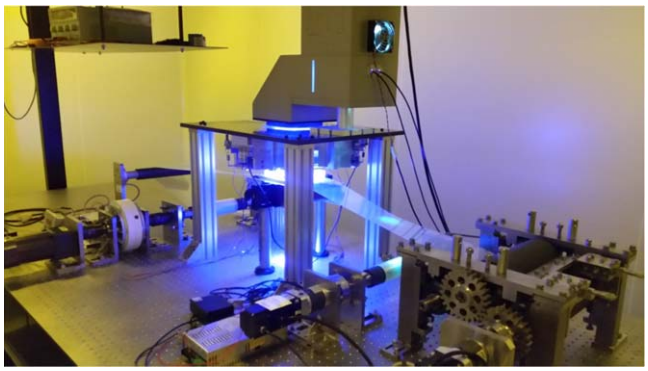

Figure 2. View of P2RNIL equipment with UV exposure.

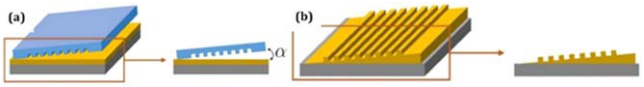

Figure 3. (a) Angular misalignment between template and substrate. (b) Imprint result due to angular misalignment.

be in parallel contact in order to avoid distortion and damage. The imprint head is driven by a tripod arrangement of three linear actuators, each of which is integrated with a linear encoder and grating ruler to provide controllable pressure and position feedback. At the very beginning, the positions of the three actuators are adjusted until the surface of the template is horizontal. During the moving-down process, a proportional-integral-derivative (PID) controller is used to move the actuators towards a specific position by reading feedback from a grating ruler. The precision of the actuator is limited by the grating ruler and can be controlled to within 1 μm. There is a vacuum chunk connected to the imprint head, through a compliant mechanism called a flexural joint, to fix the template on the lower surface. This flexural joint can be deformed passively when the template and the substrate are not in parallel contact during the imprinting process. Compared with rigid linkages, a flexural joint can generate smooth motion and avoid problems caused by friction, as long as the motions do not exceed the metal fatigue.

When the template and substrate are in contact, the flexure stage can passively adjust the level of the template. At the same time, the flexible substrate will deform passively and attain full contact. A UV light is then turned on to cure the imprint resist (as shown in figure 2). The intensity of our UV exposure is measured to be 160 mW cm^{-2} (as measured by power meter, CNI LP100). The resist can be cured in less than 2 s. The total time for a whole imprinting process is about 10 s. After a single run, the wind-up roller starts rotating while keeping the tension of the flexible substrate until the next imprint region is in place. The maximum area which can be replicated in a single run with perfectly transferred patterns is about 15 cm $\times$ 15 cm.

2.2. Design and simulation of the flexural joint.

In the imprinting process, it is essential to bring the template and substrate into parallel contact. Figure 3 illustrates an

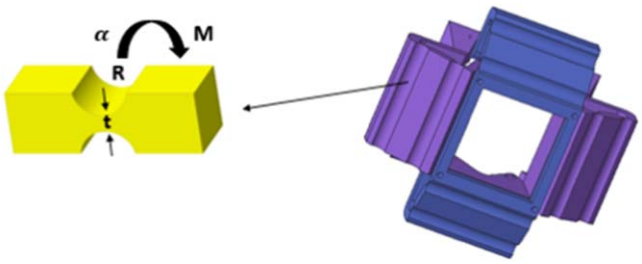

Figure 4. Structure of flexural joint and single-axis circular flexure hinges.

angular misalignment α between the template and the substrate. Such a misalignment introduces a wedge-shaped etch barrier and eventually leads to pattern loss, so the misalignment should be corrected before the etch barrier is cured. In addition, any lateral motions produced at the calibration stage should be minimized or controlled to within an acceptable range. Therefore, the P2RNIL tool should be able to correct the angular misalignment between the template and substrate, and minimize lateral or shear motions between the two surfaces. To solve the problems elaborated above, a new orientation stage based on flexure hinges is designed to hold the template so as to maintain parallel contact while minimizing relative lateral motions. Compared with the conventional technologies, stages developed by flexure mechanisms can provide smooth motion through deformations of circular flexure hinges and avoid the aforementioned problems. During the passive parallel alignment, the pressure loaded on the template is transferred to the flexural joints. When the flexural joints undergo stress, they will perform a relative rotation and displacement due to the deformation. Therefore, the compliant mechanism will correct the misalignment and minimize the lateral motion between the template and the substrate.

Combined with the kinematic feature, a flexural joint consisting of circular flexure hinges was designed. The detailed dimensions of the circular flexure hinge, which incorporates a circular cut on either side of the blank hinge, are shown in figure 4. According to the pressure needed for imprinting, the spring stiffness of every flexure hinge can be calculated by $k = M/\alpha$, where M is the moment along one direction and α is the rotation angle. Many formulas have been derived to calculate the stiffness of a flexure hinge, but most of them have their own application scope due to differing approximation methods. Lobontiu's equation [22] was chosen since it is suitable for hinges with *t/R* in the range 0.05 to 0.6, and has a low average error of 1.2%. Aluminum alloy 7075 was chosen as the design material, with a Young's modulus (E) of 71.7 GPa, for its high stiffness, good fatigue strength and good machinability. The flexure hinge was designed so that it would rotate about 0.0004 radians under a 4 N load. Based on this condition and the equation before, suitable values of t and R were calculated and picked, which are about 0.4 mm and 8 mm. Then the flexural joint (as shown in figure 4) was designed based on these parameters.

A finite element analysis was performed to verify the performance of the designed flexural joint. The upper surface of the flexural joint was fixed in the model. Forces of different

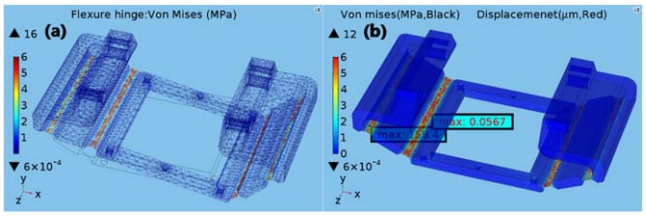

Figure 5. (a) The stress chromaticity diagram of the flexural joint. (b) The maximum stress and displacement of the flexural joint.

values were applied to the edge of the joint, to simulate the contact force when there is a small initial misalignment between two flat surfaces. Figure 5 shows the deformation and the displacement of the whole structure under a 5 N load. According to figure 5(b), the displacement of the lower surface in the x or y direction is less than 15 nm ($x_d = displacement \times \sin\theta = 56.7\ \text{nm} \times \sin 15^\circ \approx 14.7\ \text{nm}$, where θ represents the angle between the lever of the flexural joint and the surface of the template). This tiny deformation error meets the requirement for high-resolution pattern transfer. According to the stress chromaticity diagram of the flexural joint shown in figure 5(a), it is evident that the stress is concentrated at the cross-section of minimum thickness where the two axes are located. Similar to a single-axis configuration, each flexure hinge of the two-axis serial configuration will bend about its own axis. Due to the orthogonality of the axes of the flexure hinges, this design makes it possible for two adjacent rigid members to perform the relative rotation about their own axes independently.

2.3. Fabrication of the WGPs

A four-inch silicon wafer was used as our master template. By utilizing electron-beam lithography (JEOL 6300FS) and plasma etching, nanoscale patterns were fabricated on the wafer. During this process, ARP6200 was chosen as the photoresist. Silicon was etched with SF6 and C4F8 by using inductive coupled plasma (ICP) etching (Oxford ICP180). The patterns were transferred from the silicon wafer to a same-size quartz wafer by using plate-to-plate nanoimprint lithography. Then the quartz wafer was soaked in a 1H,1H,2H,2H-perfluorodecyl trichlorosilane solution for about 10 min to form an anti-sticking layer which can reduce the surface energy of the template. A top-down scanning electron microscopy (SEM) picture and cross-sectional image of 75 nm linewidth gratings are shown in figure 6.

After the P2RNIL process, cured UV resist on the PET was slightly etched with Ar and O_2 by using reactive ion etching (RIE, Oxford NGP80). The linewidth of the gratings can be narrowed down to about 30 nm. Then, 50 nm of Al was thermally evaporated onto PET at oblique angles and WGPs based on flexible substrate were finally achieved.

2.4. Fabrication of the TME.

Different from WGPs, an imprinting process named UV-assisted metal transfer imprinting was developed to fabricate TME structures. The process flow is shown in figure 7.

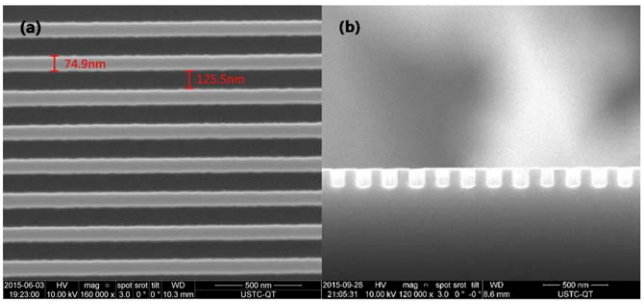

Figure 6. (a) Top-down SEM picture of the template. (b) Cross-sectional SEM picture of the template.

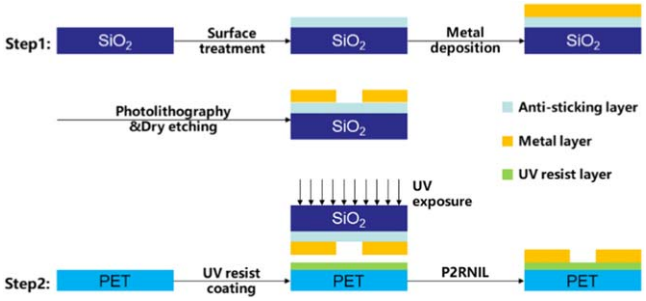

Figure 7. Process flow of UV-assisted metal transfer imprinting.

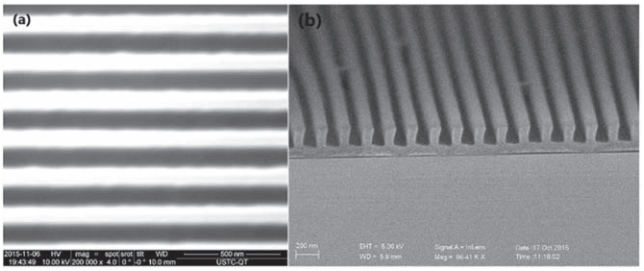

Figure 8. (a) Top-down SEM picture. (b) Cross-sectional SEM picture of imprint results on the flexible substrate.

Surface treatment was firstly performed on the surface of a four-inch quartz wafer to form an anti-sticking layer, using the same method as described above, and 800 nm Al was then deposited on it. After that, photolithography was used to define mesh patterns on the quartz wafer. By using the photoresist as a mask, patterns can be transferred to the metal layer through an ICP etching process (Oxford ICP180). The template was then soaked in methylpyrrolidone solution for 20 min to remove the residual resist.

By performing the same P2RNIL process, metal mesh was directly transferred from the template onto the flexible substrate. The adhesion difference in each surface played a critical role in successful transfer.

3. Results and discussion

3.1. The properties of fabricated WGPs

Imprinted gratings with 75 nm linewidth were achieved as shown in figures 8(a), (b). For the P2RNIL process, the template is peeled off parallel to substrate orientation during the demolding process, which allows a much lower separation force compared with conventional NIL. A lower separation force reduces the probability of defects being generated.

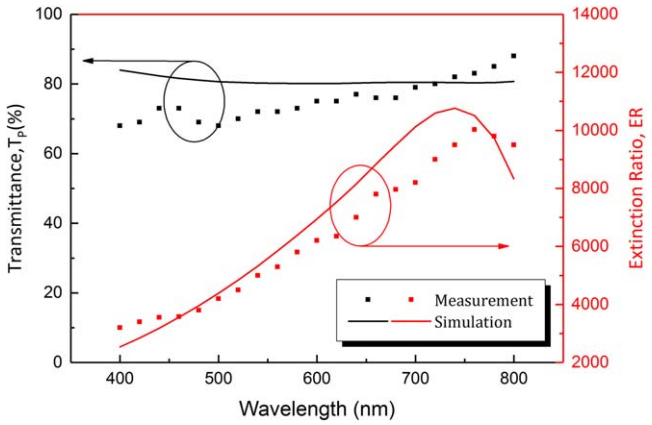

Figure 9. Simulated and measured transmittance and extinction ratio of WGPs fabricated by P2RNIL process.

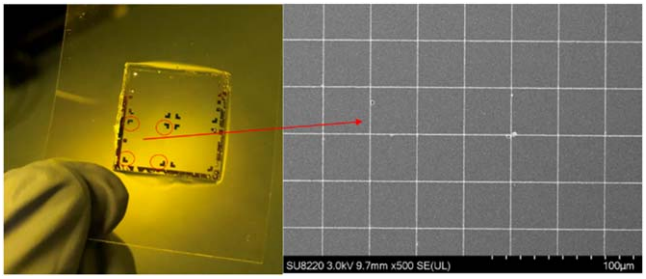

Figure 10. Fabricated TME on flexible substrate.

The WGPs fabricated by the P2RNIL process achieved a high optical transmittance of up to 88% and a high extinction ratio (ER) of up to 10 030:1 over a wide spectrum range (from 400 nm to 800 nm), as shown in figure 9. Key parameters such as linewidth and pitch can affect both the transmittance and ER of a WGP. To understand how it works, Finite-difference time-domain method solutions were used to model the optical behavior of a three-dimensional gratings structure. It shows that the transmittance and ER value drops as the linewidth and pitch are increased. For a given pitch, while the ER is largely enhanced by increasing the linewidth, there is an overall decrease of transmittance, which is more apparent at a 500 nm spectrum band. As shown in figure 9, when the linewidth and pitch are 75 nm and 200 nm, the simulated optical properties agree very well with the measured results (measured by spectrophotometer, SolidSpec-3700).

3.2. The properties of fabricated TME

TME structures were successfully fabricated on flexible substrate, as shown in figure 10. There are four regions consisting of periodically arranged metal mesh structures with 600 nm linewidth and 33 um period. Each region is surrounded by L-type electrodes, as marked in red circles, and they have the same dimensions of 1 cm × 1 cm. It is worth

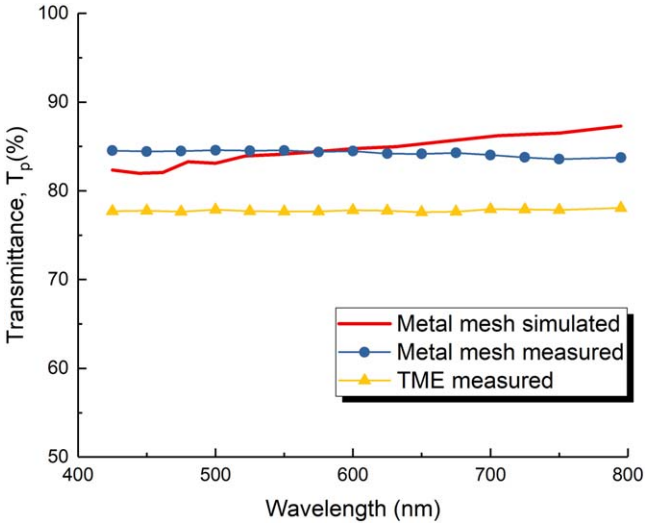

Figure 11. Simulated and measured transmittance of metal mesh.

mentioning that there was no pattern loss during the imprinting process, and the imprinted mesh structures showed good uniformity over the whole area.

To characterize the sheet resistance of the TME, an electric current as low as 1 mA was applied on two adjacent L-type electrodes in a single region. The voltage drop was then detected between the other two electrodes, which turned out to be 1.3 mV, and the sheet resistance can be calculated according to the formula $R_s = \frac{2\pi}{\ln 2} \cdot \frac{\Delta V}{I}$; that is, 11.78 Ω/□ [23]. The conductivity of the TME can be enhanced by increasing the linewidth and the thickness of the metal bar, but with lower transmittance.

The optical transmittance of the TME as measured by spectrophotometer is shown in figure 11. The fabricated TME has a transmittance of about 78% and is consistent in a spectrum range from 400 nm to 900 nm. Since TME is a combination of metal mesh and flexible substrate, the transmittance of the metal mesh itself can be measured by setting the transmittance of PET as a baseline. The results show that the transmittance of the metal mesh is 84%. The simulated results agree very well with the measured value.

In summary, we have successfully fabricated WGPs and TMEs with high performance by using a self-designed P2RNIL system. This system offers great potential in the manufacture of the flexible devices widely demanded in flexible electronics.

Acknowledgments

This work is supported by the fundamental research for central universities No. WK2030380008; National Science Foundation of China grant Nos. 61775206 and 61590932. The fabrication work was partially carried out at the USTC Center for Micro and Nanoscale Research and Fabrication.

ORCID iDs

Liang Wang https://orcid.org/0000-0003-2422-0916

References

[1] Lee S-M, Kwon J H, Kwon S and Choi K C 2017 A review of flexible OLEDs toward highly durable unusual displays *IEEE Trans. Electron Devices* **64** 1922–31
[2] Pagliaro M, Ciriminna R and Palmisano G 2008 Flexible solar cells *ChemSusChem* **1** 880–91
[3] Park S, Vosguerichian M and Bao Z 2013 A review of fabrication and applications of carbon nanotube film-based flexible electronics *Nanoscale* **5** 1727–52
[4] Sergan T, Lavrentovich M, Kelly J, Gardner E and Hansen D 2002 Measurement and modeling of optical performance of wire grids and liquid-crystal displays utilizing grid polarizers *J. Opt. Soc. Am.* A **19** 1872–85
[5] Yu X J and Kwok H S 2003 Application of wire-grid polarizers to projection displays *Appl. Opt.* **42** 6335–41
[6] Chou S Y, Krauss P R and Renstrom P J 1995 Imprint of sub-25 nm vias and trenches in polymers *Appl. Phys. Lett.* **67** 3114–6
[7] Guo L J 2007 Nanoimprint lithography: methods and material requirements *Adv. Mater.* **19** 495–513
[8] Chou S Y, Krauss P R and Renstrom P J 1996 Imprint lithography with 25 nanometer resolution *Science* **272** 85–7
[9] Ahn S H and Guo L J 2008 High-speed roll-to-roll nanoimprint lithography on flexible plastic substrates *Adv. Mater.* **20** 2044–9
[10] Ahn S H and Guo L J 2009 Large-area roll-to-roll and roll-to-plate nanoimprint lithography: a step toward high-throughput application of continuous nanoimprinting *ACS Nano.* **3** 2304–10
[11] Schift H 2006 *Roll Embossing and Roller Imprint Science and New Technology in Nanoimprint* (Japan: Frontier Publishing) p 74
[12] Kooy N, Mohamed K, Pin L T and Guan O S 2014 A review of roll-to-roll nanoimprint lithography *Nanoscale Res. Lett.* **9** 320
[13] Tan H, Gilbertson A and Chou S Y 1998 Roller nanoimprint lithography *J. Vac. Sci. Technol. B* **16** 3926–8
[14] Hauser H, Michl B, Schwarzkopf S, Kübler V, Müller C, Hermle M and Bläsi B 2012 Honeycomb texturing of silicon via nanoimprint lithography for solar cell applications *IEEE J. Photovoltaics* **2** 114–22
[15] Maury P *et al* 2011 Roll-to-roll UV imprint lithography for flexible electronics *Microelectron. Eng.* **88** 2052–5
[16] Ok J G *et al* 2015 A step toward next-generation nanoimprint lithography: extending productivity and applicability *Appl. Phys.* A **121** 343–56
[17] Kim M S *et al* 2008 Choice of electrode geometry for accurate measurement of organic photovoltaic cell performance *Appl. Phys. Lett.* **92** 133301–133301
[18] Cariou R, Benick J, Feldmann F, Höhn O, Hauser H, Beutel P, Razek N, Wimplinger M, Bläsi B and Lackner D 2018 III–V-on-silicon solar cells reaching 33% photoconversion efficiency in two-terminal configuration *Nat. Energy* **3** 326
[19] Cao H *et al* 2002 Fabrication of 10 nm enclosed nanofluidic channels *Appl. Phys. Lett.* **81** 174–6
[20] Guo L J, Cheng X and Chou cf 2003 Fabrication of size-controllable nanofluidic channels by nanoimprinting and its application for DNA stretching *Nano Lett.* **4** 69–73
[21] Gao H *et al* 2006 Air cushion press for excellent uniformity, high yield, and fast nanoimprint across a 100 mm field *Nano Lett.* **6** 2438–41
[22] Lobontiu N 2002 *Compliant Mechanisms: Design of Flexure Hinges* (Boca Raton, FL: CRC Press)
[23] Miccoli I, Edler F, Pfnür H and Tegenkamp C 2015 The 100th anniversary of the four-point probe technique: the role of probe geometries in isotropic and anisotropic systems *J. Phys. Condens. Matter* **27** 223201